Muon Lifetime

Santiago R., Birge Sükrü Tok [1]
[1] *Physics Institute, Humboldt University Berlin, Deutschland*
Instructor: Dr. Marzieh Bahmani
(Abgabe: June 30, 2021; Versuchsdatum: 6.5.2021)

When cosmic rays in the form of extraterrestrial high energy particles like protons and other nuclei hit the Earths atmosphere, air showers of subsequently produced elementary particles are generated in a cascade of particle interactions and decays set loose by this initial collision. Muons are among the elementary particles produced in such events, having a very short lifetime of around $2.2\mu s$ before decaying. Using a series of plastic scintillators on the ground with different stopping layers for the particles in the air shower, the mean lifetime of these cosmic ray muons τ_μ can be computed from the measured event rates. This value was computed through statistical evaluation of the probability density $\rho(t)$ for their detection as $\tau_\mu = (2.17 \pm 0.12_{Sys} \pm 0.18_{Stat})\mu s$

I Introduction

I.1 Background and Theory

Muons (also classified as leptons) are subatomic elementary particles similar to positrons and electrons, posessing the same electric charge $\pm 1e$ and spin $1/2$, but with a much larger mass of $m_\mu = 105.658$ MeV compared to their electron peers at $m_e = 0.510998$ MeV [LM]. Muons are generated by means of the weak interaction through the following decays of charged pions

$$\pi^+ \to \mu^+ + \nu_\mu$$
$$\pi^- \to \mu^- + \overline{\nu}_\mu$$

which are in turn created by proton-proton and proton-neutron interactions during the initial collision of cosmic ray nuclei with other such particles within the atmosphere. Depending on the charge of the pions, positively or negatively charged muons are produced and these in turn decay quickly through the exchange of a W boson into either positive positrons or negative electrons as follows

$$\mu^+ \to e^+ + \nu_e + \overline{\nu}_\mu$$
$$\mu^- \to e^- + \overline{\nu}_e + \nu_\mu$$

The time between these succesive interactions - the one in which the muon itself exists as a particle and thus the lifetime- is very short and on average about $\tau_\mu \approx 2.2\mu s$. They are able to reach the ground however due to relativistic time dilation playing a role at their speeds of $v \lesssim 0.995c$. This results in a time dilation of $\Delta t \lesssim 22\mu s$, giving them enough time to descend the altitude of ~ 60km at which they are created. It remains very short however and due to this, it is challenging to measure it directly, needing instead to be inferred from the probability density function $\rho(t)$ of a muon surviving after a certain amount of time t. This probability density function (PDF for short) is yielded by the function for the number of expected muons N

$$N(t) = N_0 e^{-t/\tau_\mu} \tag{1}$$

which, as an exponential function, corresponds to a PDF of

$$\rho(t) = \frac{1}{\tau_\mu} e^{-t/\tau_\mu} \tag{2}$$

This however is for the ideal measurement situation in which all muons are counted by the scintillator detectors, which is not the case for the experimental setup used here [Subsect. 1.2]. Here, the negative muons can also be captured by the Coulomb field of positively charged atomic nuclei when going through the aluminum sheet used to stop them, thus binding them to the core as according to the reaction

$$\mu^- + p \to n + \nu_\mu$$

instead of decaying and being counted by the scintillators. This occurs at a similar timescale of μs, leading to an artificial extension of the average lifetime of the muon τ_{eff}

$$\frac{1}{\tau_{eff}} = \frac{Q}{\tau_\mu} + \Lambda_C \tag{3}$$

which needs to be compensated as follows in equation (1);

$$N(t) = N_{\mu^+} \left(e^{-t/\tau_\mu} + \frac{1}{f} e^{-t/\tau_{eff}} \right) \tag{4}$$

Here, Q and Λ_C are respectively the Huff factor and capture rate value of the material capturing the negative muons [Table 1]. Then the effect on the total amount of muons expected now also depends on the ratio of positive to negative muons $f = N_{\mu^+}/N_{\mu^-} = 1.270(3)$ indicated in [8]. Thus, the PDF now becomes

$$\rho(t) = \frac{1}{\tau_\mu} e^{-t/\tau_\mu} + \frac{1}{\tau_{eff}} \cdot \frac{1}{f} e^{-t/\tau_{eff}} \tag{5}$$

and it can be fitted through a maximum likelihood method to the data recorded in the histogram by means of a $min(\chi^2)$ fit, where the normalized, squared distance of the fitted curve from the measured values as represented by χ^2 is minimized.

I.2 Measurement Setup and Circuit Logic

Using scintilators, high energy particles may be detected utilizing Photomultiplier Tubes (PMT). In this setup, 3 layers of scintilator plates, shielded on top by a 10 cm layer of lead and a 6 cm layer of aluminum between the second and third layer of scintilators. The former serves to filter out other particles. The later further stops muons such that they may disintegrate in a controlled manner. The resultant "slow muon" or

the electron positron pair are then detects in the second and third scintilator layers.

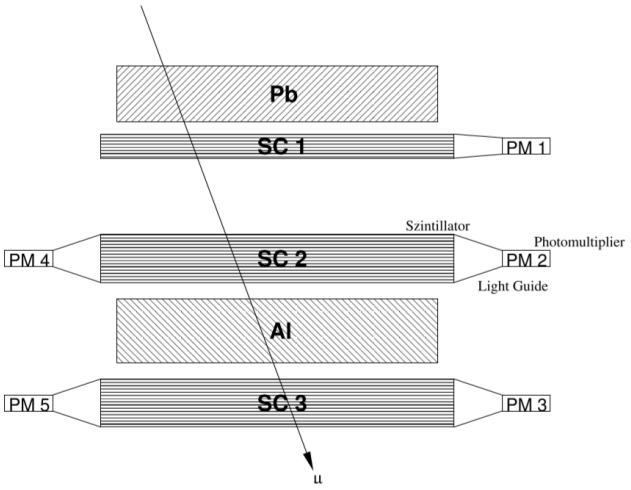

Figure 1: Schematic of Detector Setup

These layers of scintilators are outfittet with PMTs, connected through waveguides to the Scintilators. With scintilator 1 (SC1) having one and SC2 and SC3 having 2 PMTs mounted. PMT1 is mounted on SC1, PMTs 2 and 4 on SC2 and PMTs 3 and 5 on SC3. The double measurement through these 2 PMTs serves for noise reduction. To achieve this, a circuit is built using NIM modules. Prior to the signal reaching the first NIM module, the signal is converted to TTL (Transistor to Transistor Logic), a by the modules usable standard.

As a detection in any one of the SCs would need to trigger all PMTs mounted to the SC, installing a and Logic gate with the 2 mounted PMTs on SC1 and SC2, filters out most of the noise generated by the PMTs, through electron leakages and other internal random events. This leaves a clean, usable signal representing detections in the SCs. The noise in PMT1 is here not as critical, as the start-signal logic -which requires a pulse from both SC1 and SC2- as a side effect filters its noise out.

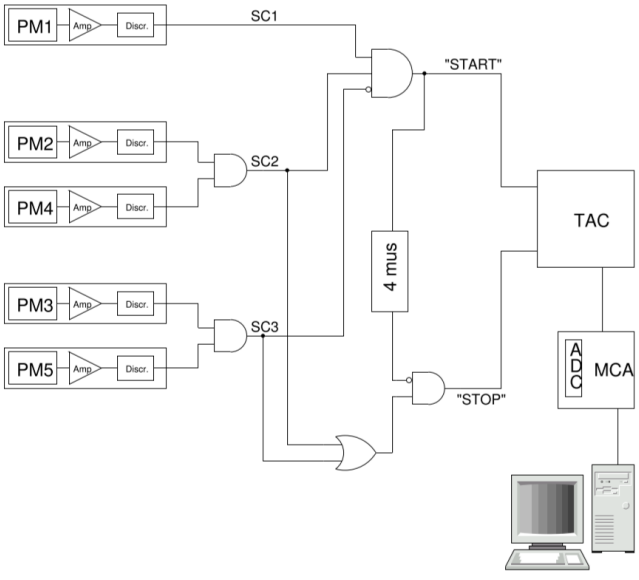

Figure 2: Circuit diagram

Since SC3 would not be triggered at the start of a detection, its inverse signal is connected to the Start-Logic-Gate. This means that SC1 and SC2 both need to be triggered, while SC3 is not for the measurement to begin. The measurement is then stopped when a detection occurs in SC2 or SC3 after a set delay of 4µs. To achieve this, SC2 and SC3 are used as inputs for an AND gate, which is then fed into an AND gate along with the inverse delay signal. This signal needs to be inverted, as the delay signal is set to "OFF" while the delay is running. Once the delay time has passed, or no detection occurred and thus delay was started, it switches to an "ON" state.

Finally, both START and STOP signals control the Time to Amplitude Converter (TAC). This device converts the measured time into an amplitude encoded signal. This is then readable by a computer with specialized software after converting the analog signal into a digital one by means of Analog to Digital Converter (ADC) at the end the signal chain.

The characteristic Huff factors and capture rates for the materials used in this setup are given by literature [2] as

Material	Λ_C	Q
Al	$(0.7054 \pm 0.0013)\mu s^{-1}$	0.993
Cu	$(5.676 \pm 0.037)\mu s^{-1}$	0.967
Pb	$(13.45 \pm 0.18)\mu s^{-1}$	0.844

Table 1: Huff factors and capture rates for the setup materials used

II Characterisation and Adjustment of the Setup

In order to verify that the detector setup, the signal chain and all components within are behaving as expected; some tests and calibrations need to be performed. Especially with regards to the delay times in the signal chain and the behaviour of the signal in different combinations of PM signal processing through gates.

II.1 Runtime Behavior of Signals

The delay caused by the coincidence modules -the modules that act as our logic gates- were measured by comparing the output signal of the coincidence unit creating its input to the output. By doing so, a further delay is introduced by the cable connecting the input generating coincidence unit to the input of the to be measured coincidence unit. This is however negligible as the delay induced by the cable is small in comparison.

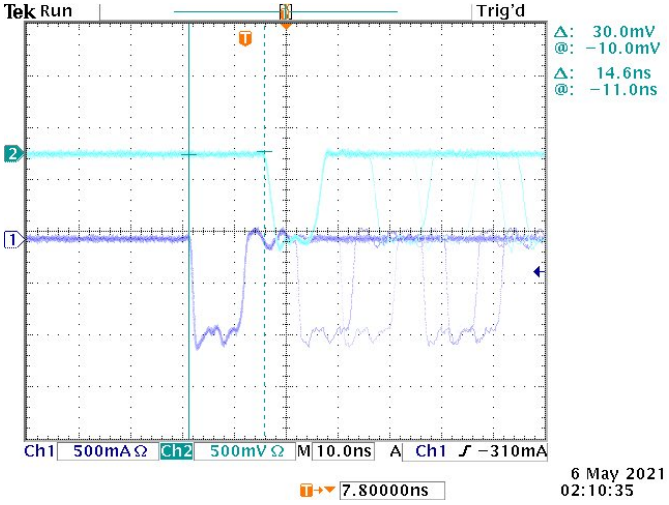

Figure 3: Sample Delay measurement, Signal from SC1, from Octal Discriminator (LeCroy 4608) output (CH1) to Coincidence unit (LeCroy465) output (CH2)

A delay of around 12-15 ns with all units was observed. Since this is multiple orders of magnitude smaller than our expected measurement value, and thus much smaller than our expected uncertainty, these delays are neglected.

During these measurements, the Lecroy 622C Quad Coincidence Logic unit showed a change in pulse width. How far this may impact the measurement, or how this may be rectified, remains to be analyzed. It is likely that since the time periods are significantly small, the resulting change in pulse width did not influence the measurements in a significant way.

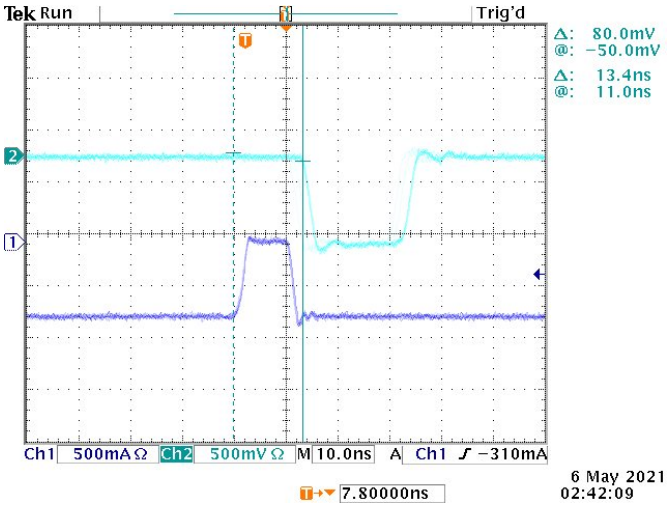

Figure 4: Delay measurement with pulse width change, Signal from SC2, from Octal Discriminator (LeCroy 4608) output (CH1) to Quad Coincidence unit (LeCroy622C) output (CH2)

II.2 Event Rates

The event rates of the PMTs as well as their combinations as Scintilators SC1, 2 and 3 with different combinations were measured using a NIM Quad Scaler module and given below in counts-per-second (cps) and counts-per-minute (cpm).

- each PMT
  - PMT1, avg: 500cps, Stdev: 41.6cpm
  - PMT2, avg: 1290cps, Stdev: 60.4cpm
  - PMT3, avg: 7736cps, Stdev: 1452cpm
  - PMT4, avg: 866cps, Stdev: 74.1cpm
  - PMT5, avg: 6794cps, Stdev: 1344cpm
- each SC
  - SC1, avg: 500cps, Stdev: 41.6cpm
  - SC2, avg: 147cps, Stdev: 14.7cpm
  - SC3, avg: 160cps, Stdev: 11.9cpm
- SC1 and SC2, avg: 14.4cps, Stdev: 4.97cpm
- SC1 and SC2 and SC3, avg: 5.25cps, Stdev: 2.45cpm
- SC1 and SC2 not SC3, avg: 11cps, Stdev: 2.68cpm
- SC2 and SC3, avg: 17.5cps, Stdev: 3.90cpm
- and finally SC2 or SC3, avg: 296cps, Stdev: 22.5cpm

A 1 second measurement was repeated 10 times for these values. The conclusion from this data is that the noise reduction within the SC assemblies works as expected. Looking at SC3, this becomes especially apparent, due to its drop in events compared to the PMTs. Furthermore, looking at SC2 and SC3, and SC2 or SC3 strengthens this conclusion, as the or gate configuration outputs about the same as the sum of the two SCs. This also visualizes how much noise is generated within the PMTs and how many irrelevant independent events take place within the SCs.

II.3 Time Calibration

In order to properly record data such that each so called channel on the X-axis may be mapped to a given time, a calibration to the TAC is necessary. This is achieved by using a single trigger signal -here SC1- as both the start and stop trigger. By means of the delay module, a top signal with a given delay -confirmed through measurement with an osciloscope- that set time is fed to the TAC. Repeating this over multiple set times, a map is generated, by mapping the given time to its respective channel with first measurement. The point of first measurement was chosen, as no lower measurements should be possible due to the fixed delays as a minimum.

When doing this, it is necessary to feed the output to the veto input of the delay module. This serves to prevent interference between independent subsequent pulses.

It would be favourable to observe the resulting TAC Pulse and determine if it is follows the expectations. Unfortunately, recording of the measurement was not possible, as the pulse duration was far too small for us to react in such a manner that the imaging stops during a pulse display. We observed the Pulses being above a certain threshold, as expected. This was at first confusing, as we expected a constant amplitude, dependant on the delay. However, since the pulse durations at the input of the TAC vary, with the minimum possible duration being the delay time. Thus the pulses observed behave as the theory would dictate.

III Measurement of the Muon Lifetime

In order to compute the mean lifetime τ_μ of the muon from the measurements, the stored data first needs to be calibrated and rebinned while also taking into account the delays and other runtime behaviors characterized during Section II. After calibrating the data, a fitting procedure can be applied in order to extract the parameter τ_μ for the muons average lifespan before decaying.

III.1 Background Signal and Delay

First, a 30 minute long measurement without any delay set in the TAC is taken to check both background signals and the need for an artificial delay of $4\mu s$. This is due to the photomultipliers used in the setup to detect any photon signals in the scintillators being very sensible, causing them to also measure a lot of background events other than the muon ones.

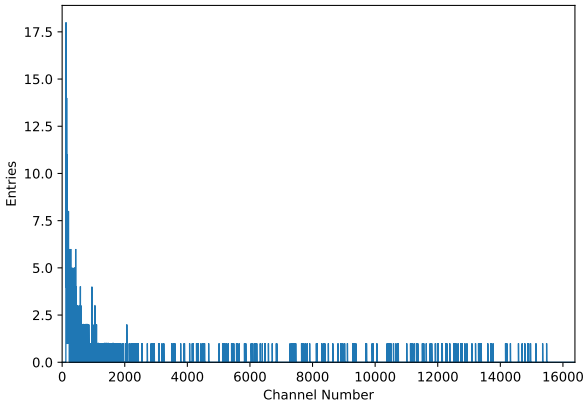

Figure 5: Histogram of a 30 minute measurement without delay

Looking at the recorded spectrum, it is noticeable that a steady signal builds up beyond the initial peaks from recorded muon events, potentially drowning out any signals from longer surviving muons. In order to reduce the amount of such false events from the subsurface that are recorded into the histogram, the artificial delay of $4\mu s$ is used to discard any stop signals coming into the TAC within those $4\mu s$ after a start signal. This heightens the probability that the recorded event is actually a muon event instead of any other one. Setting this delay and recording a measurement over several hours during the night then yields

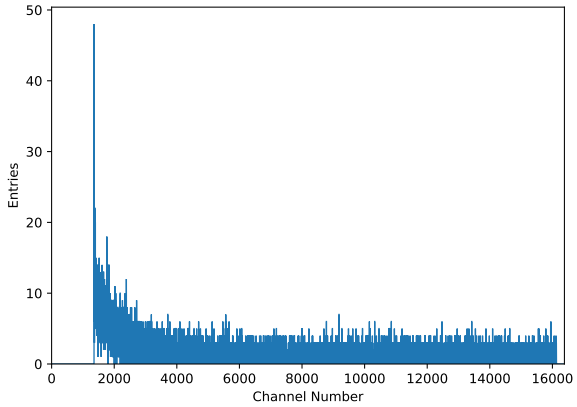

Figure 6: Histogram of an overnight measurement with a $4\mu s$ delay

Within this histogram, there is both a significant increase in the total counts recorded within the measurement, as well as a change in the overall distribution, which appears much more like an exponential decay as predicted by the theory and in contrast to the more delta-function like graph in Fig. 5. The rate at which muons are detected lies roughly in the 5-20cps ballpark as described in Section II.2 and a measuring time of about at least 16 hours is necessary for an accurate determination of the mean lifespan of the muon within 1%.

III.2 Calibration Curve

As first discussed in the time calibration section, the functional, ideally linear relationship between the channel number in the MCA and the TAC needs to be accurately computed in order to calibrate the time measurement of the histogram. Using single trigger signals as explained in Section II.3, a calibration spectrum such as the one below is produced

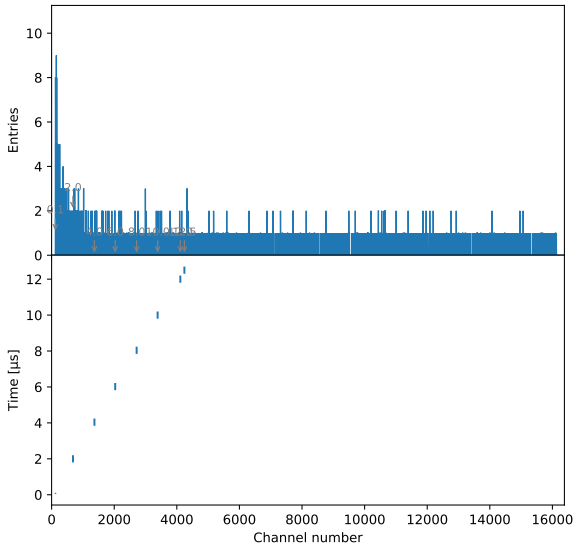

Figure 7: Combined spectrum of single trigger signals

, where the individual channels and corresponding set delay times are mapped below the spectrum, showing a roughly linear shape. The exact values are

Channel Number	Time
120 ± 5	$(0.08 \pm 0.002)\mu s$
682 ± 5	$(2 \pm 0.005)\mu s$
1367 ± 5	$(4.04 \pm 0.1)\mu s$
2031 ± 5	$(6.02 \pm 0.1)\mu s$
2716 ± 5	$(8.04 \pm 0.1)\mu s$
3387 ± 5	$(10 \pm 0.1)\mu s$
4112 ± 5	$(12 \pm 0.1)\mu s$
4242 ± 5	$(12.5 \pm 0.1)\mu s$

Table 2: Channel Numbers and Trigger Times

and when used to fit the following linear slope

$$t(x) = mx + d \tag{6}$$

through a least squares $\sum_i \left(\frac{f_i(x)-y_i}{\Delta y_i}\right)^2$ approach, the produced calibration line gives the relationship between the channel numbers x and the time t. For the values above, this yields

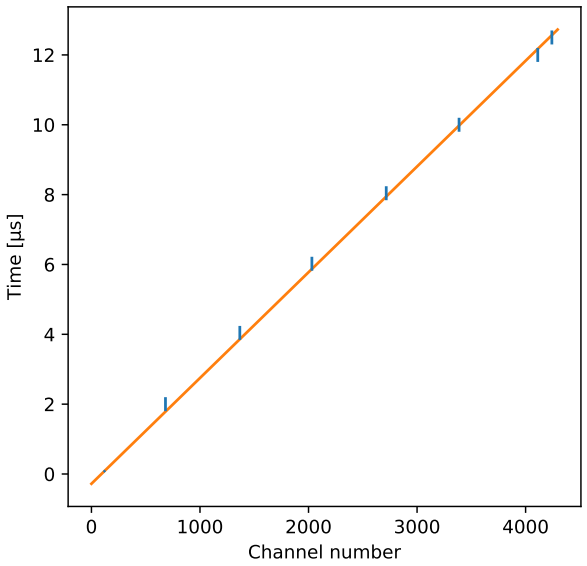

Figure 8: Calibration line fit $t(x)$

m	d
$(0.003028 \pm 0.000027)\mu s$	$(-0.279 \pm 0.021)\mu s$

Table 3: Fitted parameters

where the linear relationship between the channel numbers and registered times appear to hold up well at first glance. For a quantifiable indication of the fits quality however, the $\frac{\chi^2}{dof}$ value of the fit may be computed as well, yielding in this case a value of $\frac{\chi^2}{dof} = 0.7286$, somewhat below the ideal value of 1 for a "good" fit, and indicating either an overestimation of the uncertainty indicated above, possibly suggesting lower such uncertainties, or a need for more measurements.

III.3 Rebinning

Using the calibration line above, the raw spectrum measurement from Fig. 6 recorded overnight can now be transformed into the time domain. In addition, the counts from individual channels can also be summarized together in a numerical procedure known as rebinning, so as to allow for further averaging out of noise in the measured muon signal.

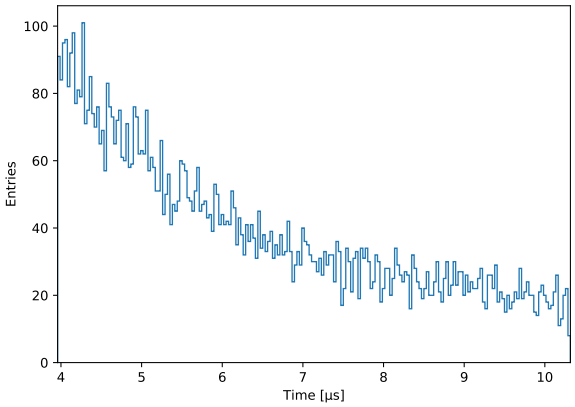

Figure 9: Rebinned and time calibrated spectrum

The rebinning starts from channel 1400 (3.92µs), which roughly corresponds to the start of the measurement after the 4µs delay, and goes up to channel 3500 (10.2µs) where the signal from the muon decays appears to drown within the noise from other events as seen in the plot without rebinning in Fig. 6. The bins essentially summarize the data and contain the average of the counts from 10 neighboring channels. These boundaries were chosen in order to fit the section with the highest signal to noise ratio, while binning together only neighboring channels with thus similar counts so as to only even out more possible sources of noise.

III.4 Determination of the mean lifetime of Muons τ_μ

After the rebinning and time calibration, it is now possible to apply a non-linear fit in order to compute the values for the mean lifetime of the muons. Based on the theory from the introduction as well as equations (4) and (5) one gets the following fit function

$$N(t) = N_{\mu^+}\left(\frac{1}{\tau_\mu}e^{-t/\tau_\mu} + \frac{1}{\tau_{eff}} \cdot \frac{1}{f}e^{-t/\tau_{eff}}\right) + C \tag{7}$$

for the rebinned spectrum in the time domain. Here, the effective lifetime τ_{eff} is given by the characteristic parameters of aluminium Λ_C and Q in Table 1 as

$$\tau_{eff} = \left(\frac{Q}{\tau_\mu} + \Lambda_C\right)^{-1} \tag{8}$$

Applying a minimizing $\chi^2 = \sum_i \left(\frac{f_i(x)-y_i}{\sqrt{f_i(x)}}\right)^2$ fitting algorithm, which is a maximum likelihood method based on a χ^2 distribution of the measured values from the

theoretical prediction, the following fit is yielded by the Python Iminuit package used for the numerical evaluation

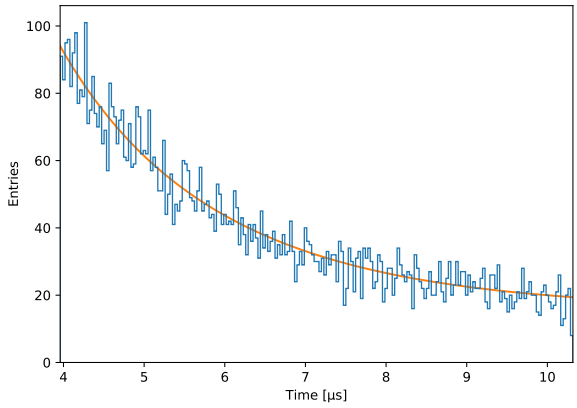

Figure 10: Fit N(t) for the rebinned spectrum, $\chi^2 = 161.5$

$N_{\mu+}$	τ_μ	C
940 ± 80	$(2.17 \pm 0.18)\mu s$	15.7 ± 1.5

Table 4: Fitted parameters

The values given above vary somewhat depending on the rebinning as well as the calibration of the spectrum. Meanwhile, the convergence of the fit is only guaranteed for certain initial guesses. The resulting parameters are within the expected bounds however, with some room for discussion regarding the systematic uncertainties in the next section. For this binning and calibration as according to the arguments above, the mean lifetime of the muon is returned by the algorithm as

$$\tau_\mu = (2.17 \pm 0.18)\mu s \tag{9}$$

III.5 Background Influences and Systematic Error Estimates

As explained in previous sections, despite many layers of noise reduction in the scintillator setup - such as time delay and rebinning for the sake of averaging out potentially noisy signals, comparing input and output signals from the different scintillators etc. - there is still a significant amount of background events capable of artificially altering the spectrum and thus systematically deviating the fitted parameters further from the actual values despite the statistic uncertainties not indicating so.

Among possible background events are thermal radiation within the scintillator, external light sources as indicated later during the discussion and also terrestrial radiation from radium, thorium and uranium in the soil, as well as airborne radiation carried mostly by radioactive gases like radon, which emanates from the radioactive decay of these elements. All these can potentially trigger the scintillator detectors and generate a false signal that if timed correctly can also be recorded into the histogram as a false muon event.

Regarding the systematic uncertainties from the time calibration and rebinning, a series of fits according to the same model function and raw data as in Section III.4 but with different values and settings for these were computed and compared. The resulting values for the relevant parameters are given in the table below

Modified Setting	τ_μ	$N_{\mu+}$
Calibration Upper Lim.	$(2.23 \pm 0.21)\mu s$	$(1000 \pm 110)\mu s$
Calibration Lower Lim.	$(2.08 \pm 0.20)\mu s$	$(890 \pm 90)\mu s$
Binning up to 8000/20	$(2.74 \pm 0.09)\mu s$	$(1570 \pm 60)\mu s$
Binning up to 16000/29	$(3.05 \pm 0.09)\mu s$	$(2100 \pm 70)\mu s$

Table 5: Fitted parameters for different Settings

Here, the settings were modified in the first two table entries such that the effect of the uncertainties in the fitted calibration parameters were taken into account by either adding (Calibration Upper Lim.) or substracting (Calibration Lower Lim.) the uncertainties prior to computing τ_μ. In the later two table entries, the binning thresholds were modified to the maximal bin channel N and bin width dN indicated in the N/dN format.

It is apparent from these values that the largest contribution to the systematic uncertainty stems from the chosen thresholds for rebinning, as choosing higher thresholds increases the fitted parameter for τ_μ, most likely due to increases in the noise to signal ratio for higher channel counts where the signal from actual muon events is lower and thus more easily drowned out by the background. Combining the deviations σ_i from the calibration through the square sums $\sum \sigma_i^2$ -as the ones from higher binning thresholds aren't relevant for the output from smaller binning thresholds where the signal to noise ratio would only improve- one gets;

$$\tau_\mu = (2.17 \pm 0.12_{Sys} \pm 0.18_{Stat})\mu s \tag{10}$$

IV Discussion

The value computed for the mean lifetime of the muon $\tau_\mu = (2.17 \pm 0.12_{Sys} \pm 0.18_{Stat})\mu s$ is in good agreement with the expected value from the literature [2] of $\tau_{Lit} = 2.19703(4)\mu s$. This lies within the expected result from an overnight collection of muon events and also further confirms the validity of the linear relationship assumed for the time calibration of the channel values, despite the somewhat low value of the reduced $\frac{\chi^2}{dof} = 0.7286$ indicating that the uncertainties may have been overestimated or further measurements were required for a better calibration.

Regarding the binning, a large amount of the measured events were essentially discarded by choosing the 1400-3500 channel threshold mentioned, which was estimated by visual observation of the signal to noise ratio in the raw spectrum from figure 6. This indicates that there were still a noticeable amount

of background events affecting the measurement at lower signal levels from the muon events, as discussed in Section III.5.

Furthermore, during a preliminary run of event rate measurement, with the blinds on the windows up, the measurements for SC3 and its PMTs were 5-6 times the values of measurements with the blinds down and the room darkened. This shows that some photons do still leak in through the shielding on the sides, and that the shielding installed may not be sufficient to rule out all particles entering the detector setup from the side. It is possible that side shielding needs to be expanded due to this.

V References

[1] Fundamental Physical Constants; National Institute of Standards and Technology; June 30, 2021; https://physics.nist.gov/cgi-bin/cuu/Value?esme

[2] Dr. Marzieh Bahmani: *Measurement of the muon lifetime* , 2021